An Automatic Diagnostic System for CT Liver Image Classification

E-Liang Chen, Pau-Choo Chung,* *Member, IEEE*, Ching-Liang Chen, Hong-Ming Tsai, and Chein-I Chang, *Senior Member, IEEE*

***Abstract*— Computed tomography (CT) images have been widely used for liver disease diagnosis. Designing and developing computer-assisted image processing techniques to help doctors improve their diagnosis has received considerable interests over the past years. In this paper, a CT liver image diagnostic classification system is presented which will automatically find, extract the CT liver boundary and further classify liver diseases. The system comprises a *detect-before-extract* (DBE) system which automatically finds the liver boundary and a neural network liver classifier which uses specially designed feature descriptors to distinguish normal liver, two types of liver tumors, hepatoma and hemageoma. The DBE system applies the concept of the normalized fractional Brownian motion model to find an initial liver boundary and then uses a deformable contour model to precisely delineate the liver boundary. The neural network is included to classify liver tumors into hepatoma and hemageoma. It is implemented by a modified probabilistic neural network (PNN) [MPNN] in conjunction with feature descriptors which are generated by fractal feature information and the gray-level co-occurrence matrix. The proposed system was evaluated by 30 liver cases and shown to be efficient and very effective.**

***Index Terms*— Fractal, liver boundary, probabilistic neural network, segmentation.**

I. Introduction

DUE to the advent of computer technology, image processing techniques have become increasingly important in a wide variety of applications. This is particularly true for medical imaging such as ultrasonography, computed tomography (CT), magnetic resonance image (MRI), and nuclear medicine which can be used to assist doctors in diagnosis, treatment, and research [1]. According to recent statistics [2], liver cancer is one of leading cancerous diseases in Taiwan. Therefore, designing and developing computer-aided diagnostic (CAD) tools for liver cancer is of particular interest in Taiwan. Thus far, the only definitive test for liver cancer is needle biopsy. However, the needle biopsy is an invasive technique and generally not recommended unless there is an absolute need. To avoid unnecessary needle biopsy, doctors can take advantage of information provided by images acquired from various medical imaging systems such as surface texture, object boundary extraction, tumor detection, etc. to assist them to improve their diagnosis. In this case, an effective image analysis is important. Although many segmentation methods have been successfully used in medical imaging, it has found that most of them generally do not perform well in segmenting the liver boundary from a CT liver image. This is mainly due to the fact that there are other organs adjacent and close to the liver which makes segmentation more difficult. In addition, the liver itself may also contain tumors such as hepatoma and hemageoma that can obscure the boundary. In order to address these problems, we present an automatic CT liver image classification system which can be used to detect two types of liver tumor: hepatoma and hemageoma.

As a first step of extracting liver tumors, we need to isolate or segment the liver boundary within a CT liver image. A novel approach called the "*detect-before-extract*" (DBE) technique is proposed for this purpose. Since the liver is generally accompanied by other organs which presents difficulties for liver boundary segmentation, DBE decomposes the process into two stages. The first stage processing is boundary detection and then followed by a second stage processing, boundary extraction. The detection procedure can be implemented as follows. It first transforms the original CT liver image into a binary-valued normalized fractional Brownian (NFB) feature bit map from which a region growing technique is used to find an initial liver boundary. It is generated by dividing an original image into a set of 16×16 image blocks and assigning either a zero or one to each of the image blocks. This binary value is determined according to its corresponding NFB feature curve. More precisely, each point in the feature bit map represents a 16×16 image block. A point assigned by a one indicates that its represented image block is considered as part of the liver region. On the contrary, a zero-value point means that its represented image block is not part of the liver region. Using such zero-one NFB feature bit map, an initial boundary of the liver region can be delineated. Since each point in the NFB feature bit map is actually a 16×16 image block, the detected initial liver boundary needs to be interpolated back in the original image domain. This interpolation is done by a Catmull–Rom B-spline. Since the interpolated liver contour may not be precise, it is further refined and corrected by a deformable model. The

Manuscript received November 8, 1995; revised December 14, 1997. The work of P.-C. Chung and C.-I Chang was supported by the National Science Council (NSC) under Grants NSC 84-2213-E-006-087 and NSC 84-2213-E-006-086, respectively. *Asterisk indicates corresponding author.*

E-L. Chen and C.-L. Chen are with the Department of Electrical Engineering, National Cheng Kung University, Tainan, Taiwan 70101, R.O.C.

*P.-C. Chung is with the Department of Electrical Engineering, National Cheng Kung University, Tainan, Taiwan 70101, R.O.C. (e-mail: pcchung@eembox.ee.ncku.edu.tw).

H.-M. Tsai is with the Department of Radiology, Medical College and Hospital, National Cheng Kung University, Tainan, Taiwan 70101, R.O.C.

C.-I Chang is with the Department of Computer Science and Electrical Engineering, University of Maryland Baltimore County, Baltimore, MD 21250 USA.

Publisher Item Identifier S 0018-9294(98)03719-7.

resulting liver boundary will be considered to be the desired liver boundary.

As soon as the desired liver boundary is generated, a texture feature-based classification system is then applied to discriminate two types of liver tumors: hepotoma and hemageoma. The classification system is developed based on a modified probabilistic neural network (PNN) [MPNN] classifier which includes the Kohonen self-organization algorithm to reduce the number of training patterns. The inputs to the MPNN are a set of feature descriptors that are generated by gray-level co-occurrence matrices and a NFB motion model. According to studies [3], it was found that statistically, the hepatoma, a malignant tumor, is usually more coarse-grained, while the hemageoma, a benign tumor, has more homogeneous textures, though the texture difference in these two types of disease images may not be easily observed by human eyes. In addition, the hemageoma usually has higher gray-level intensity and contrast than hepatoma. In order to capture the unique texture characteristics of hepatoma and hemageoma, several feature descriptors derived from NFB motion model and co-occurrence matrix such as contrast, homogeneity, entropy, and energy, are particularly designed for this purpose. Finally, the proposed complete CT liver image classification system combines the DBE system with the MPNN classifier to achieve automatic liver boundary extraction and liver tumor classification. In order to see the effectiveness, the system is tested and evaluated by 30 liver cases. The results are encouraging and show promise of the system.

This paper is organized as follows. Section II reviews the concept of the NFB motion model and defines the NFB feature curves. Section III describes a novel idea, "*detect-before-extract*" for liver boundary segmentation. Section IV modifies the Specht's PNN classifier to classify two types of liver tumor: hepatoma and hemageoma. Finally, a brief conclusion is included in Section V.

II. Normalized Fractional Brownian Motion Model Feature Curves

The concept of fractal was first introduced by Mandelbrot [4] who used it as an indicator of the surface roughness. It was later applied by Pentland [5] to natural scene analysis and by Keller [6] for textured image segmentation with the gray level replaced by the fractal dimension (FD). In particular, the FD has been used in image segmentation for an index to measure surface roughness where different natural scenes such as mountains, clouds, trees, and deserts generate different FD's. While the fractal concept is useful in various applications, different fractal models were also proposed in the past. Among them is the fractional Brownian motion (FBM) model [7] which has shown promise. It represents random walks which can be used to model the randomness reflected by organ structures and inherent random noises. As a result, the FBM model is a nature adoption in medical imaging for analysis. For example, in [8] and [9], the feature vectors generated by image blocks based on a NFB motion model were used to classify normal and abnormal ultrasonic liver images.

A. Fractional Brownian Motion Model

In [4] Mandelbrot and Van Ness described FBM as a nonstationary self-affine random process. Nonetheless, the increments of FBM is a strict-sense stationary process, called a fractional Gaussian noise (FGN) with probability distribution given by a Gaussian random variable with zero mean and variance specified by

$$\mathrm{var}[B(x+\Delta x)-B(x)] = V_H \cdot ||\Delta x||^{2H} \tag{1}$$

where V_H is a constant determined by $0 < H < 1$ and $B(x)$ is the FBM at random walk x [4].

If the image intensity I is described by the FBM model with parameter H, then the increment $\Delta I_x = |I(x_2) - I(x_1)|$ is Gaussian distributed with zero mean and variance given by $C \cdot ||\Delta x||^{2H} = C \cdot ||x_2 - x_1||^{2H}$, or more precisely

$$E\left[\Delta I_x^2\right] = C \cdot ||\Delta x||^{2H} \tag{2}$$

where $E[\cdot]$ denotes the statistical expectation operator and C is a constant. Equation (2) can be also rewritten as

$$E\{|\Delta I_x|\} = \bar{C} \cdot ||\Delta x||^{H} \tag{3}$$

where $\bar{C}$ is also a constant determined by C. Taking the logarithm on both sides of (3), we obtain

$$\log E[|\Delta I_x|] = H \cdot \log ||\Delta x|| + \log \bar{C}. \tag{4}$$

Since both $\bar{C}$ and H are constants, we can plot $\log E[|\Delta I_x|]$ versus $\log ||\Delta x||$ in the log-log domain. The resulting curve is called the fractional Brownian feature curve. If the FBM can be used to describe a surface, H must be a constant for all Δx. The slope of the curve, denoted by H, can be estimated by a least squares linear regression. The FD of the image is then obtained as $D = 3 - H$. A smaller value of FD D indicates a smoother surface, while a larger D means a rougher surface.

B. Normalized Fractional Brownian Feature Curves

As mentioned previously, the concept of FBM model has been used in feature extraction to describe the roughness of nature surface. Given an $N \times N$ image I, an intensity difference vector of the image I is defined as $IDV \equiv [id(1), id(2), \cdots, id(s)]$ where s is the maximum possible scale and $id(k)$ is defined as follows:

$$\begin{aligned} id(k) &= \Bigg[\sum_{x=0}^{N-1} \sum_{y=0}^{N-k-1} |I(x,y) - I(x,y+k)|/N(N-k) \\ &\quad + \sum_{y=0}^{N-1} \sum_{x=0}^{N-k-1} |I(x,y) - I(x+k,y)|/N(N-k) \\ &\quad + \sum_{x=0}^{N-k-1} \sum_{y=0}^{N-k-1} |I(x,y) - I(x+k,y+k)|/(N-k)^2 \\ &\quad + \sum_{x=0}^{N-k-1} \sum_{y=0}^{N-k-1} |I(x,N-y) - I(x+k,N \\ &\quad - (y+k))|/(N-k)^2 \Bigg] \Big/ 4 \end{aligned} \tag{5}$$

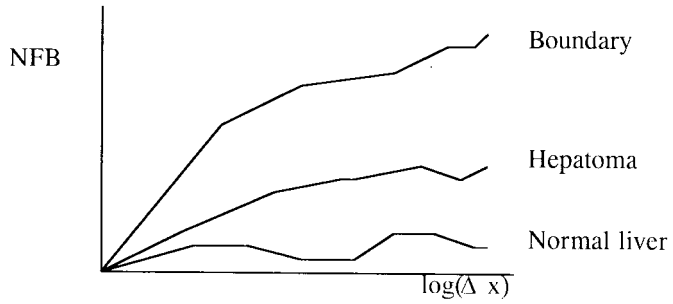

Fig. 1. NFB feature curve obtained from our experimental result.

where all pixel pairs calculated in the absolute difference in (5) are k-pixel apart along horizontal, vertical, diagonal, and asymmetric-diagonal directions. The NFB motion feature vector NFB is then obtained from the *IDV* through (5). Namely, $NFB = [f(1), f(2), \cdots, f(k), \cdots, f(n)]$ with

$$f(k) = \log(id(k)) - \log(id(1)), \quad k = 1, 2, \cdots, n. \qquad (6)$$

For an intensity surface described by the FBM, $id(k) = C(\Delta x_k)^H$ with a constant C and $f(k) = H\log(\Delta x_k) - H\log(\Delta x_1) = H\log(\Delta x_k/\Delta x_1)$. If $\Delta x_1 = 1$, $f(k) = H\log(\Delta x_k)$ is invariant to C. This implies that $f(k)$ is invariant to any linear intensity transformation.

In this paper, the NFB motion feature vector will be used to classify three types of regions in a CT liver image, normal liver, hepatoma, and liver boundary (or complexity region). An example is shown in Fig. 1 where three averaged NFB feature curves were plotted for normal liver, hepatoma, and liver boundary, respectively. Since the normal liver has smooth texture, its corresponding curve is flat as expected. When a liver area has hepatoma, the rough texture of hepatoma results in a steep NFB curve. Because the boundary area usually covers different organs, its texture is generally complex. Therefore, the resulting NFB curve must have a very high slope to represent such a phenomenon. Fig. 1 shows these three curves are well separated. As a consequence, they can be used for liver boundary segmentation and hepatoma/hemageoma classification as will be seen in Sections III and IV. However, for the purpose of quantitative study, we will use the NFB feature values, which are calculated by the areas under the NFB feature curves, rather than the curves themselves.

III. A Detect-Before-Extract Method for Finding Liver Boundary

Finding and detecting the boundary detection of CT liver images is important in medical diagnosis. An accurate liver boundary not only provides doctors with the liver contour information, but also offers preliminary knowledge with which doctors can determine whether or not further image processing needs to be done such as filtering, enhancement, analysis and three-dimensional visualization.

Since the liver is generally accompanied by other organs, a direct liver-extraction approach without preprocessing may also extract unwanted boundaries resulting from its adjacent organs. In order to cope with this problem, we present a two-stage algorithm for CT liver boundary detection, called "*detect-before-extract*" process, viz., detection is done prior to extraction. It decomposes the task of liver boundary extraction into two functional procedures. The first stage is boundary detection and the second stage is boundary extraction. More specifically, the "*detect*" procedure is to find an initial silhouette of the liver boundary by transforming an original image into a binary-valued NFB feature bit map. It is then followed by an "*extract*" procedure to interpolate and refine the obtained initial liver contour and further extract the desired liver boundary from the original image. Generally speaking, the first stage of the "*detect before extract*" strategy can be thought of as an initial liver contour finding procedure which uses the NFB feature bit map in conjunction with a region growing method to locate the initial liver boundary. The second stage of the "*detect before extract*" strategy is a liver boundary extraction process which applies a deformable contour model to interpolate and refine the initial liver boundary obtained in the first stage so that an accurate delineation of the liver boundary can be extracted. This proposed *detect-before-extract* method has proven to be effective and efficient in most of our experiments.

A. Initial Liver Boundary Detection

As mentioned previously, the purpose of finding the initial liver boundary is to keep track of the liver boundary while avoiding possible inclusion of unwanted objects. If the initial contour is too far away from the liver boundary, it might be very difficult to accurately extract the liver boundary. By doing so, a texture-based region growing method is proposed to automatically locate the initial liver contour. The idea is to find unique texture features which can distinguish the liver from other organs such as kidney, gastrointestinal tract, and spinal cord, then use them as a base for region growing. These features can be generated as follows.

First of all, a CT image is divided into $M \times N$ regions, R_{ij} where $i = 1, \cdots, M$ and $j = 1, \cdots, N$. From *a priori* knowledge, the liver cannot be located in the right-bottom area of a liver image. So, the regions in this area cannot be part of the liver and can be eliminated so as to reduce the search area for liver boundary. Next, for each of the remaining regions R_{ij}, two feature values will be calculated, the average gray level, denoted by $\bar{G}_{ij}$ to form an average gray-level map (AG map), and the average feature value, denoted by F_{ij}, obtained from the NFB model to form an average feature map (AF map).

Based on the results of Section II, each feature value F_{ij} provides important information: normal liver $(F_{ij} \leq 0.1)$ or hepatoma $(0.1 \leq F_{ij} \leq 0.3)$, or liver boundary (otherwise). According to the values of F_{ij} in the AF map, each region R_{ij} can be classified into one of three classes: normal liver class, hepatoma class, or liver boundary class (or complexity region). Let C_{nl} be the normal liver class containing all the regions R_{ij} with $F_{ij} \leq 0.1$, and C_h be the hepatoma class made up of regions R_{ij} with $0.1 \leq F_{ij} \leq 0.3$. For the normal liver and hepatoma classes, their class means are calculated.

Let μ_{nl} be the mean of the normal liver class given by

$$\mu_{\mathrm{nl}} = \frac{\sum_{R_{ij} \in C_{\mathrm{nl}}} \bar{G}_{ij}}{N_{\mathrm{nl}}}$$

where N_{nl} is the number of total regions belonging to the normal liver class. Similarly

$$\mu_h = \frac{\sum_{R_{ij} \in C_h} \bar{G}_{ij}}{N_h}$$

where N_h is the number of total regions belonging to the hepatoma class. Using the means of these two classes as classification criteria, one can classify all considered regions into either the liver region or nonliver region. If a region R_{ij} is part of liver region, set $F_{ij} = 1$. Otherwise, $F_{ij} = 0$. As a result, the original image will be transformed into an NFB feature bit map. Each point of the map represents a region (i.e., an image block) either belonging to the liver or not. This liver/nonliver region classification procedure is briefly described below.

Algorithm for Generating an NFB Feature Bit Map:

If $(f_{ij} \leq 0.1$ & $|\bar{G}_{ij} - \mu_{\mathrm{nl}}| < \varepsilon_1)$ then $F_{ij} = 1$,
else if $(0.1 \leq F_{ij} \leq 0.3$ & $|\bar{G}_{ij} - \mu_h| < \varepsilon_2)$ then $F_{ij} = 1$,
otherwise $F_{ij} = 0$.

where $\varepsilon_1, \varepsilon_2$ are tolerance thresholds to indicate how much deviations to be allowed from class means.

Fig. 2(a) illustrates this feature bit map transformation. Each point in the map represents a 16×16 image block. A point labeled by "1" indicates that the image block is designated as part of the liver. As expected, the obtained initial liver region is only a reduced-size silhouette of the liver and may contain small hollows and narrow isthmuses which result from the tumors and the interferences of other organs inside the liver image. In order to take care of this artifact problem, mathematical morphological operations are applied to smooth the contours of an image, break narrow isthmuses, and eliminate protrusions [10]. The structuring elements to be used in the opening operation for morphological dilation and erosion are particularly designed for this purpose and defined in Fig. 3(a)–(d). The resulting liver region from the opening operation is shown in Fig. 2(b). Comparing to Fig. 2(a) without the opening operation, we can see that the undesired effects have been removed or smoothed.

Since the liver region is represented by a $(0, 1)$ value-based NFB feature bit map, it must be converted back to the original gray-level based image by interpolation. To emphasize the difference between the original image and feature bit map, the term "point" is reserved for an element in the NFB feature map and "pixel" for an element in the original image. After the NFB feature bit map of the liver region is generated, an interpolation technique is needed to transform back the obtained liver boundary points into liver boundary pixels in the original image.

The proposed interpolation method is to first identify all boundary points of the liver region in the NFB feature bit map, then apply a Catmull–Rom B-spline to interpolate the found NFB-feature value liver boundary to find an initial liver boundary. A point B is called a boundary point if any neighborhood centered at B contains at least one point with value one as well as at least one point with value zero. (For instance, a neighborhood can be viewed as a disc with center B and a positive integer radius $r > 0$.) Occasionally, it may be the case that a point satisfies the boundary condition but occurs in a hollow inside the liver area. So, this point will not be considered to be a boundary point and will be removed. Using these found boundary points from the NFB feature bit map as interpolative points, an initial liver contour in the original image can be generated by a Catmull–Rom B-spline. Since a point in the NFB feature bit map is defined as an image block, it will be regarded as the center of the block when it is interpolated. As a result, the interpolated liver boundary may slightly different from the original liver region. In order to fix this problem, the liver boundary is dilated using the structure elements given by Fig. 3(e)–(f) before interpolation.

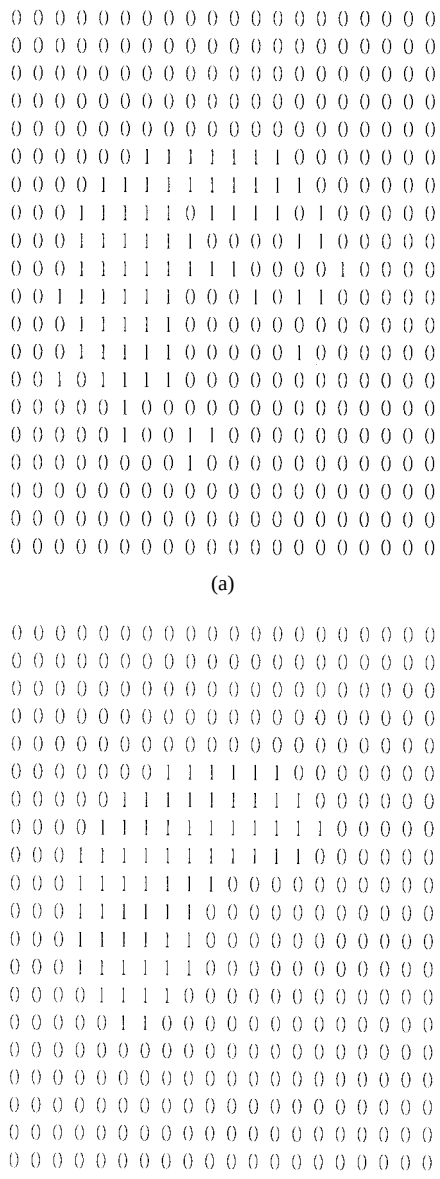

(a)

(b)

Fig. 2. The feature bit maps before and after morphological operations. (a) Before morphological operation. (b) After morphological operation. Each digit in both maps represents a 16×16 image block of the original image. The block labelled "1" is designated as a part of the liver.

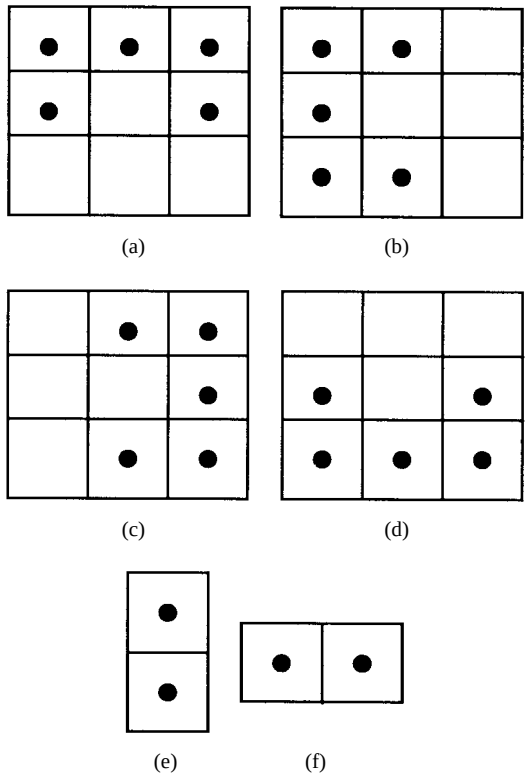

Fig. 3. (a)–(d) The structuring elements of morphological opening operations used to break narrow isthmuses, eliminate protrusions and smooth the liver contour as shown in Fig. 2. Parts (e) and (f) are the structuring elements of morphological dilation operation used before the interpolation procedure.

Fig. 4 shows that the location of the liver region of a CT image can be properly identified. However, the contour may still slightly deviate from the actual boundary. In this case, a deformable contour model is suggested to further adjust and modify the liver boundary.

B. Contour Modification Using a Deformable Active Model

As noted above, the initial liver boundary contour interpolated by a B-spline only provides a preliminary knowledge about the liver boundary. It needs to be refined and modified to find the real and actual boundary. This can be done by using a deformable contour model to iteratively correct the initial liver boundary subject to a set of constraints. The constraints required for the deformable contour model are determined by 1) the NFB feature curves F_{ij} of each pixel located at position (i,j) and 2) the difference between the gray level of the pixel G_{ij} and the averaged gray level $\mu_{\rm nl}$ of the normal liver region, i.e., the gradient value $|G_{ij} - \mu_{\rm nl}|$.

To implement this process, sample pixels are selected from the initial liver contour with n-pixel apart. For each sample pixel, a one-dimensional search line segment centered at this pixel is created and normal to the liver contour, i.e., perpendicular to the contour outward from the inside of the liver (see Fig. 5 where B represents a boundary pixel, an "x" represents an inner pixel and an "o" is an outer pixel.) Each search line segment has length of seven pixels and contains three inner pixels labeled by x's and three outer pixels labeled by o's with respect to the contour as shown in Fig. 5. For each pixel at position (i,j) in the search line segment, its corresponding NFB feature value, F_{ij} is calculated for contour modification. The window to be used for the NFB feature values is of size 7×7. Similarly, the window to be used for its gradient value, S_{ij} calculated by the Sobel operator has size 3×3. In order to determine the best boundary pixel, denoted by B^*, in each search line segment, three constraints used for a deformable model are prioritized in order as follows.

Constraints Prioritized in Order: Let $\varepsilon > 0$ be a tolerance threshold.

1) The pixel B^* is reset to the first pixel which satisfies $F_{ij} > \varepsilon$ in the search line segment starting from the innermost pixel to outer pixels.
2) The pixel B^* is reset to the first pixel which satisfies $|G_{ij} - \mu_{\rm nl}| > \varepsilon$ in the search line segment starting from the innermost pixel to outer pixels.
3) The pixel B^* is reset to the first pixel which satisfies $S_{ij} > \varepsilon$ in the search line segment starting from the innermost pixel to outer pixels. If all the pixels in the search line segment do not satisfy this condition, the pixel B^* is set to the last outer pixel of the search line segment.

Since *NFB* feature values can detect the differences among normal liver, hepatoma, and liver boundaries, the first constraint on the value F_{ij} is considered to be the most important. Thus it will be used in the first iterative process to generate a new contour that will be insensitive to hepatoma. The second constraint on G_{ij} is used in the second iterative process to separate the obtained liver contour from other organs. Finally, the third constraint on the value S_{ij} is used in the third iterative process to determine the precise location of liver boundary. Furthermore, because the liver contour is generally smooth, the sampled pixels must be properly selected. This can be done by calculating the curvatures along the contour. If a part of the contour has too large curvature, it will be replaced by an interpolated curve using a Catmull–Rom B-spline. The points used for interpolation are chosen to be the neighboring pixels of the replaced contour. The contour is modified iteratively with above prioritized constraints until the contour is stable. The algorithm can be summarized as follows.

Algorithm for Contour Modification:

1) Select proper sample pixels with n-pixel apart from the initial liver contour.
2) Form a 7-pixel search line segment across every sample pixel with three pixels inside and three pixels outside of the liver contour.
3) Find the best fitting boundary pixel in each search line segment in accordance with prioritized constraints.
4) Smooth the resulting liver contour from Step 3).
5) Interpolate the contour obtained by Step 4) using a Catmull–Rom B-spline.
6) Repeat Steps 1)–5) until the contour is stable.

Fig. 6 shows the final liver contours for three patient cases. The results show that the liver contours are accurately extracted and located. The segmentation results obtained by the above algorithm are better than that by traditional methods. In addition, in order to improve texture classification, the

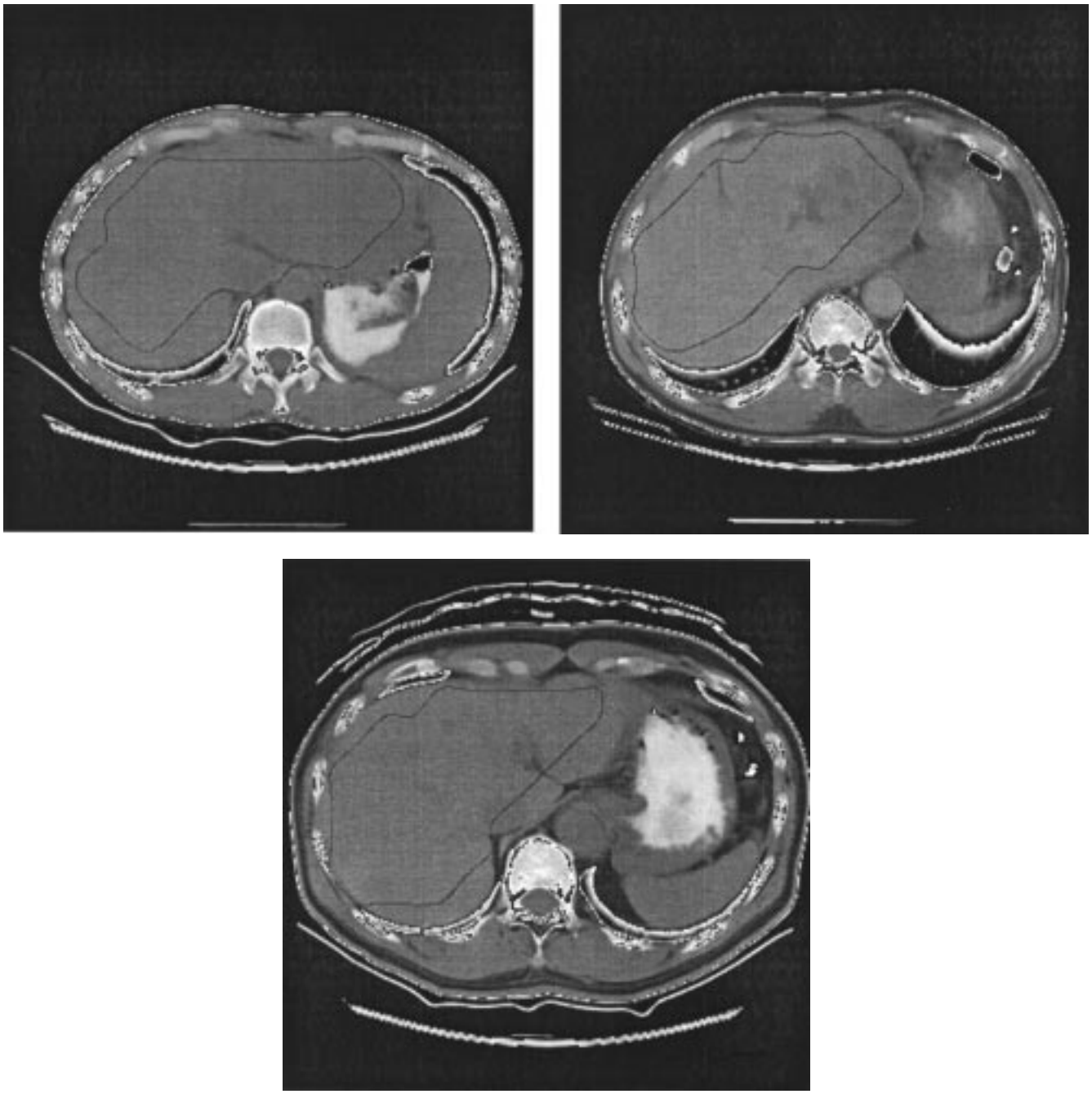

Fig. 4. Initial liver contours of three patients.

liver areas surrounded by contours are further enhanced by histogram equalization. (see the examples shown in Fig. 7). It is important to note that the whole process is automated.

IV. Classification for Liver Tumors

Using CT liver images as a diagnostic tool becomes increasingly important in liver medical modalities. However, the effectiveness is largely reduced due to a lack of applicable image processing techniques. As a result, it still relies heavily on experienced and skillful doctors. In order to improve doctors' diagnoses, a statistical texture classification system using a MPNN [11] is suggested for classification of hepatoma and hemageoma. The textures to be used for inputs of MPNN are fractal features and features generated by various spatial gray-level co-occurrence matrix (SGLCM)-based feature descriptors.

A. Spatial Gray-Level Co-Occurrence Matrices

SGLCM has been widely used in texture classification [9], [12]. Comparing to an image gray-level histogram, the SGLCM is a second-order gray-level statistic which takes into account the spatial correlation between a pair of two gray levels. Specifically, let $P(i,j;d,\theta)$ denote the transition probability from gray level i to gray level j defined by (7) shown at the bottom of the next page, where notation "$\angle$" denotes the angle between (k,l) and (m,n), $||(k,l) -$

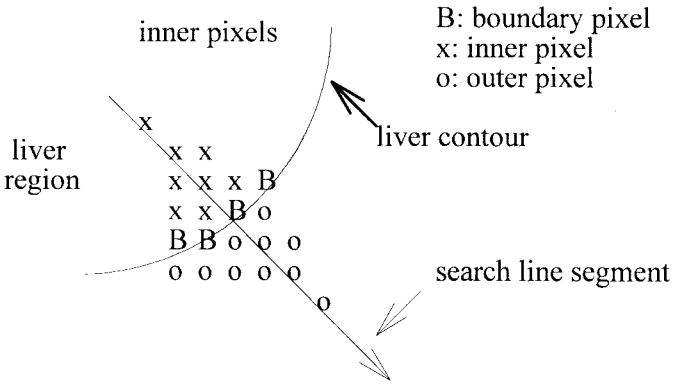

Fig. 5. Search line segment.

$(m,n)|| = d$ indicates that (k,l) and (m,n) are d-pixel apart, # is the number of elements in the set, L_x and L_y are the horizontal and vertical spatial domains, $I(x,y)$ is the image intensity at point (x,y), and $N(d,\theta)$ is the total number of pixel pairs in the image having angle θ with d-pixel apart. So, the SGLCM $M(d,\theta)$ is defined as a matrix of which the (i,j)-th entry given by $P(i,j;d,\theta)$

$$M(d,\theta) = [P(i,j;d,\theta)]_{L\times L} \tag{8}$$

where $L-1$ is the largest gray level used in the image.

From (9), if the texture of a surface is rough, the corresponding $M(d,\theta)$ is nearly diagonal. This is because for coarse textures pixel pairs separated at a small distance d usually have close gray levels which implies that $P(i,j;d,\theta)$ is high for $i \approx j$. On the other hand, $M(d,\theta)$ is sparse for fine textures since neighboring pixel pairs generally have distinct gray levels that can describe subtle differences in a small neighborhood.

In what follows, a set of six texture feature descriptors are generated based on $M(d,\theta)$ and can be used as inputs to the MPNN for classification.

Let

$$\mu_x = \sum_{i=0}^{L-1} i \sum_{j=0}^{L-1} P(i,j;d,\theta) \tag{9}$$

$$\mu_y = \sum_{j=0}^{L-1} j \sum_{i=0}^{L-1} P(i,j;d,\theta) \tag{10}$$

$$\sigma_x^2 = \sum_{i=0}^{L-1} (i-\mu_x)^2 \sum_{j=0}^{L-1} P(i,j;d,\theta) \tag{11}$$

$$\sigma_y^2 = \sum_{j=0}^{L-1} (j-\mu_y)^2 \sum_{i=0}^{L-1} P(i,j;d,\theta). \tag{12}$$

Then, the six texture feature descriptors are defined as follows.

1) Contrast:

$$con\ (d,\theta) = \sum_{i=0}^{L-1}\sum_{j=0}^{L-1} (i-j)^2 P(i,j;d,\theta). \tag{13}$$

2) Energy:

$$E(d,\theta) = \sum_{i=0}^{L-1}\sum_{j=0}^{L-1} P(i,j;d,\theta)^2. \tag{14}$$

3) Entropy:

$$H(d,\theta) = -\sum_{i=0}^{L-1}\sum_{j=0}^{L-1} P(i,j;d,\theta)\log P(i,j;d,\theta). \tag{15}$$

4) Correlation:

$$C(d,\theta) = \frac{\sum_{i=0}^{L-1}\sum_{j=0}^{L-1}(i-\mu_x)(j-\mu_y)P(i,j;d,\theta)}{\sigma_x\sigma_y}. \tag{16}$$

5) Local Homogeneity:

$$L(d,\theta) = \sum_{i=0}^{L-1}\sum_{j=0}^{L-1} \frac{1}{1+(i-j)^2} P(i,j;d,\theta)^2. \tag{17}$$

6) Sum Entropy:

$$SE = -\sum_{k} p_{\rm sum}(k)\log p_{\rm sum}(k)$$

where

$$p_{\rm sum}(k) = \sum_i \sum_j P(i,j,d,\theta) \quad \text{with } i+j=k. \tag{18}$$

It should be noted that in all conducted experiments, we have chosen $d=1$ and $\theta = 0^\circ, 45^\circ, 90^\circ$, and 135° .

B. Modified Probabilistic Neural Network (MPNN)

Neural networks have shown promise in pattern classification and considered to be a potential alternative approach to

$$P(i,j,d,\theta) = \frac{\#\{((k,l),(m,n)) \in (L_x\times L_y)\times(L_x\times L_y) : \angle(k,l)(m,n) = \theta, ||(k,l)-(m,n)|| = d, I(k,l)=i, I(m,n)=j\}}{N(d,\theta)} \tag{7}$$

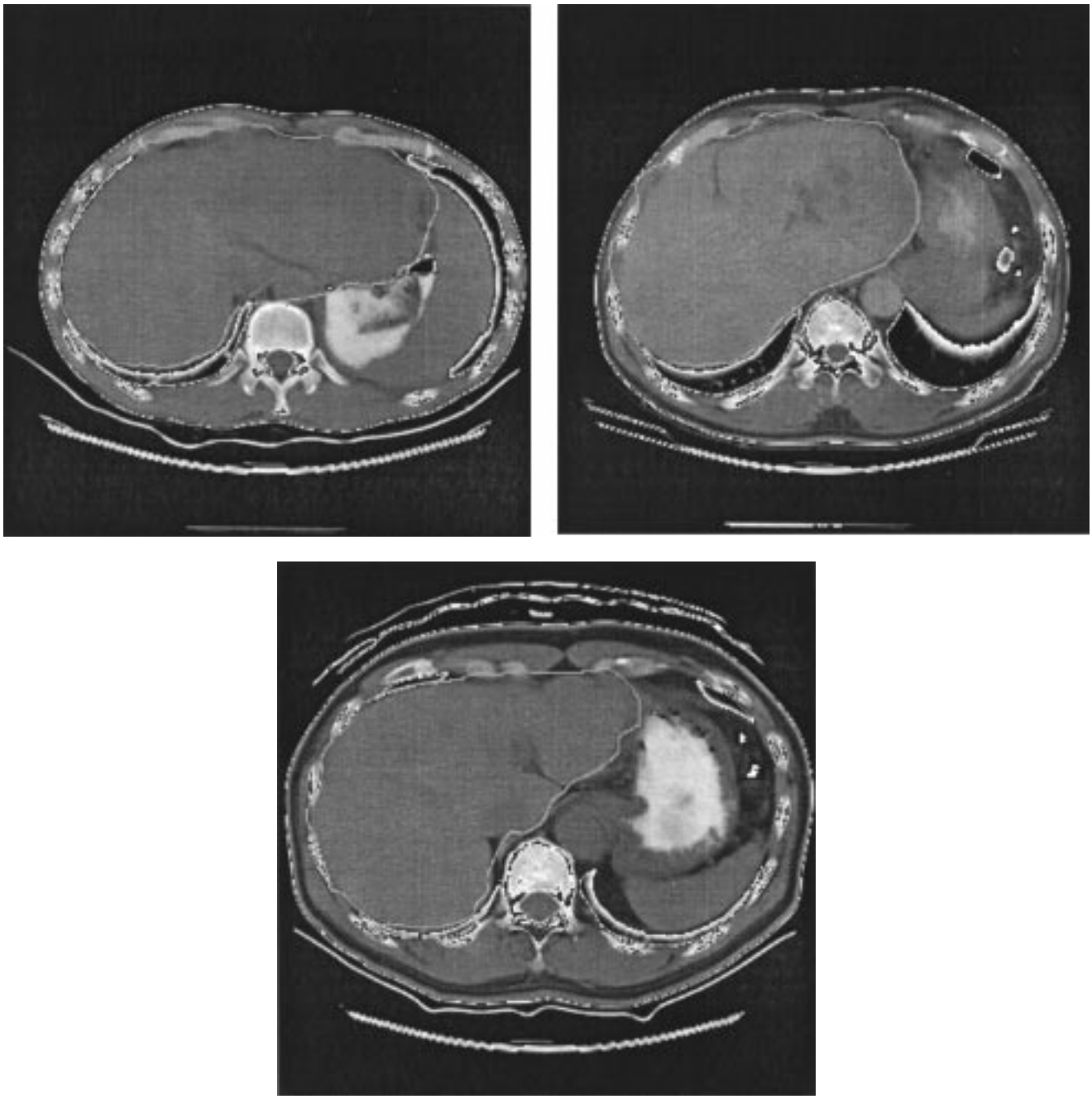

Fig. 6. Final liver contours of three patients.

statistical pattern classification. They differ from conventional approaches in that they possess learning capability and adapts themselves to rapid changing environments. Various models for neural networks have been studied in the literature, each of which has its own merit depending upon applications. Of particular interest is Specht's PNN [11] which is a Bayesian classifier and can be considered to be an optimal classifier in terms of the minimization of total misclassification risk.

In Specht's approach, the sigmoid activation function was replaced with an exponential function to realize a statistical nonlinear decision function. Let $X_1, X_2, \cdots, X_m$ be sample patterns belonging to a class and independent realizations of a random variable X with the probability measure given by P. Assume that the cumulative distribution function $F(x) = P[X \leq x]$ is absolutely continuous. If P is Gaussian distributed, the probability density function of a two-dimensional random vector $\mathbf{X}$ is given by

$$f(\mathbf{X}) = \frac{1}{m} \sum_{i=1}^{m} \frac{1}{(2\pi)\sigma^2} \exp\left[-\frac{(\mathbf{X} - \mathbf{X}_i)^T (\mathbf{X} - \mathbf{X}_i)}{2\sigma^2} \right]. \quad (19)$$

The parameter σ used in (19) is a smooth parameter used to describe the sharpness of each sample pattern distribution. According to Specht's PNN, each sample pattern requires a

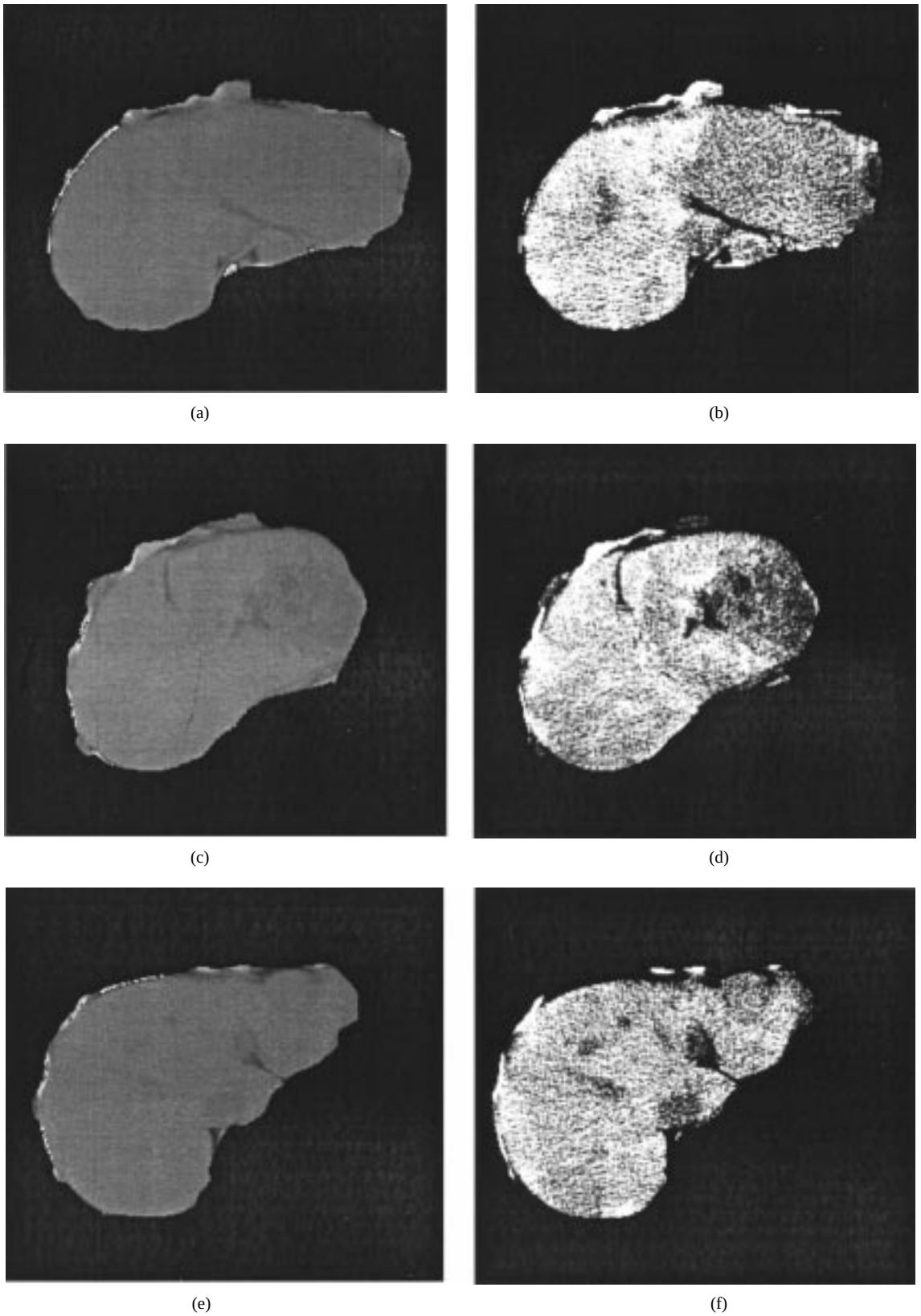

Fig. 7. The images before and after histogram equalization. (a), (c), and (e) Before histogram equalization. (b), (d), and (f) After histogram equalization.

node, i.e., represents a realization of one cluster. Therefore, as the number of training samples increases, so does the network size. This eventually makes the network prohibitive in practical applications. As such, Specht's PNN is slightly modified for this purpose by including a clustering algorithm into network design. Different patterns with slight variations in a class are grouped into clusters by means of the Kohonen learning rule. A similar approach was also suggested in [13].

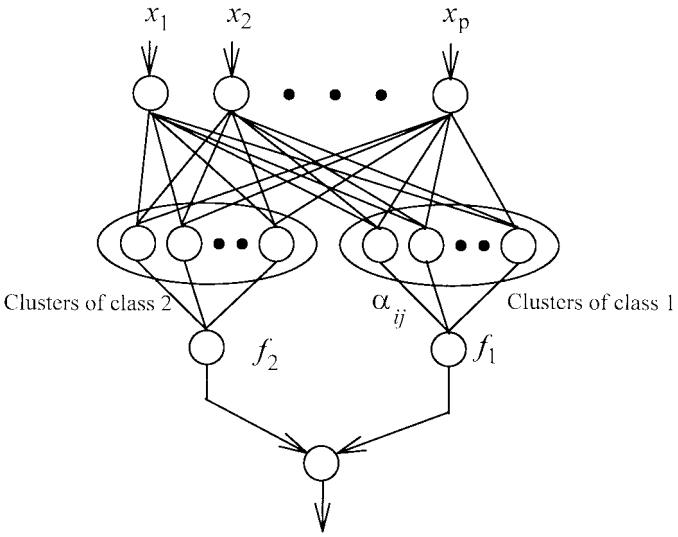

Fig. 8. The network for classification of patterns into two categories. $f_1(X)$ is the probability of X belonging to class 1—Hepatoma. $f_2(X)$ is the probability of X belonging to class 2—Hemageoma. X is the input vector which denotes the pattern.

For an input pattern X belonging to class i, a winning cluster c is selected from class i based on the following criterion:

$$||X - w_{ic}|| = \min_j \{||X - w_{ij}||\} \tag{20}$$

where w_{ij} represents the weight vector of cluster j in class i.

In order to ensure that the winning cluster can legitimately represent the pattern X, the similarity distance defined by (20) between X and w_{ic} needs to be further examined. If the distance exceeds a prescribed threshold, the cluster c will be chosen to be the representative of X; otherwise, X will be considered as a new cluster center and a new neuron will be assigned to it.

For a winning cluster w_{ic}, the Kohonen learning rule adjusts its weight vector according to the following equation given by

$$w_{ic}(t+1) = w_{ic}(t) + \alpha_{ic}(X - w_{ic}(t)). \tag{21}$$

The probability density function of class i is a mixture of probability density functions each of which representing a probability density of one winning cluster with nonnegative mixing factor α_{ic}. If the probability distributions are Gaussian, the defined probability distribution is known as a Gaussian mixture. Based on the mixture probability distribution, the decision can be easily made by choosing the class with the maximum probability, i.e., maximum likelihood estimation. Fig. 8 shows the network architecture for classification of input patterns into two categories-hepatoma and hemageoma.

C. Experimental Results

All the CT images used in the following experiments were acquired from the hospital of National Cheng Kung University (NCKU) by a GE 9800Q CT scanner at spatial resolution 10 mm and were stored in a 486/33-Hz PC. Each acquired image has the spatial resolution of 320×320 pixels with 12 bits representing 4096 gray levels. All the hepatoma cases considered in this experiment were validated by needle biopsy and all the hemageoma cases were followed up for more than two years. The algorithms used were written by C language. Fig. 9(a) and (c) shows the images having hepatoma and hemageoma, respectively, while Fig. 9(b) and (d) shows their corresponding NFB curves. For each acquired image, a block of 16×16 pixels is selected to produce an NFB feature bit map. All the texture feature descriptors used for classification are described in Section III. From our experiments, it has been found that the features obtained from NFB motion, i.e., the shape vector of the NFB curve is the best among all the feature descriptors described by (13)–(18). The shape vector of the NFB curve is defined as $SV = [s(1), s(2), \cdots, s(n)]$ where n is the maximum possible scale and $s(i)$ is the area between $i-1$ and i under the NFB curve. In order to reduce the effect of blocking artifacts resulting from the noise in the block or the inhomogenity of the block, the NFB curve is calculated by averaging its four neighboring blocks. The correlation and sum entropy of SGLCM defined by (16) and (18) show better performance than the other feature descriptors. As a result, these three feature descriptors, i.e., shape vector of the NFB, correlation of SGLCM, and sum entropy of SGLCM were used as inputs to MPNN for classification of hepatoma and hemageoma. In the MPNN, all the features obtained from NFB, correlation and sum entropy are normalized.

TABLE I
CONFUSION MATRIX IN THE CT LIVER CLASSIFICATION

Correct class \ Classified as	H	M
H	17	3
M	2	8

H = hepatoma
M = hemageoma.

The determination of the σ parameter is also important in classification. Since only two groups need to be classified, a larger value of σ was used in our experiments. The data used in the experiments comprises 20 patients with hepatoma and ten patients with hemageoma. The classification rate is about 83%. The confusion matrix is given in Table I. Some misclassifications have nothing to do with the proposed system but result from tumors which are smaller than a 16×16 block size. This is due to the fact that the block size used to generate the NFB feature bit map is too large. So, the classification rate can be increased by reducing the block size.

V. CONCLUSION

A system based on fractal geometry and MPNN was developed for the CT liver image classification. The system consists of an automatic liver contour extraction process, an image enhancement algorithm and a hepatoma/hemageoma classification network. During the process of liver contour extraction, the liver area is first located using the fractal feature values, then followed by a deformable contour model to iteratively generate the accurate liver contour. With the help of the deformable contour model, the liver contour can precisely be extracted. After the liver area is extracted,

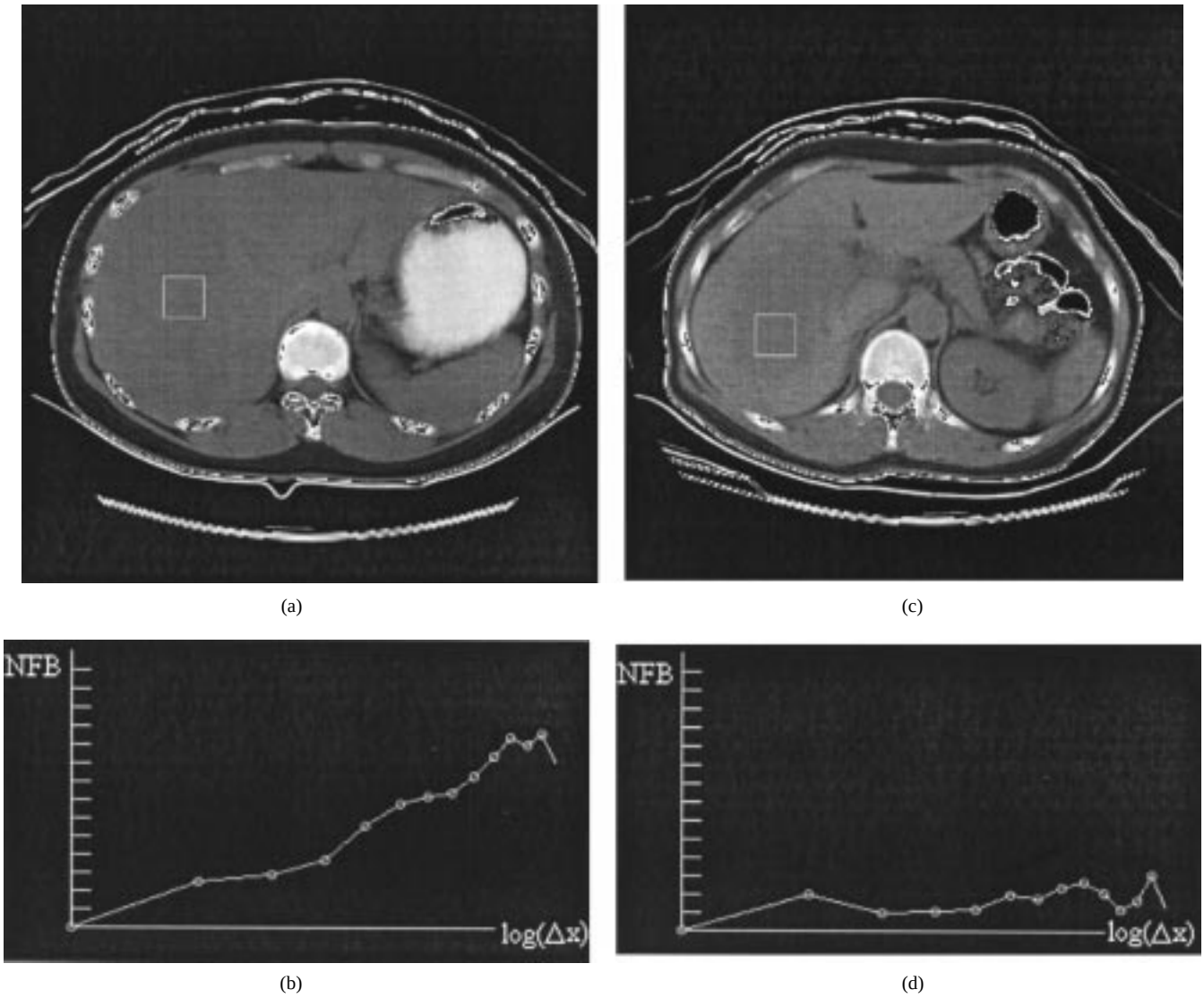

Fig. 9. The hepatoma and hemageoma images and their NFB curves. (a) The image of hepatoma. (b) The NFB curve of the selected hepatoma block in (a), and Δx = pixel distance. (c) The image of hemageoma. (d) The NFB curve of the selected hemageoma block in (c), and Δx = pixel distance.

it will be further enhanced for future feature texture-based classification. Our experiments show that using the NFB feature values, the correlation and sum entropy of the spatial gray-level dependence matrices in conjunction with a MPNN has better performance in classification than using other feature descriptors in MPNN. It should be noted that the MPNN used in this paper is not necessarily optimal in all applications. It can be replaced by any classification system as long as it performs better than MPNN. This shows that the designed system is object-oriented. In other words, any component in the system can be replaced by a better system if there exists one.

REFERENCES

[1] J. P. Heiken, P. J. Wegman, and J. K. T. Lee, "Detection of focal hepatic masses: Prospective evaluation with CT, delayed CT, CT during arterial portography, and MR imaging," *Radiology*, vol. 171, pp. 47–51, 1989.
[2] J. L. Sung, T. H. Wang, and J. Y. Yu, "Clinical study on primary carcinoma of the liver in Taiwan," *Amer. J. Digestive Diseases*, vol. 12, no. 10, pp. 1036–1049, 1967.
[3] O. H. Wegener, "Whole body computerized tomography," English translated by J. H. Long. Berlin, West Germany: Schering AG, 1983.
[4] B. B. Mandelbrot and J. W. Van Ness, "Fractional Brownian motions, fractional noises and applications," *SIAM Rev.*, vol. 10, no. 4, pp. 422–437, 1968.
[5] A. Pentland, "Fractal-based description of natural scenes," *IEEE Trans. Pattern Anal. Machine Intell.*, vol. PAMI-6, pp. 666–674, 1984.
[6] J. M. Keller, S. Chen, and R. M. Crownover, "Texture description and segmentation through fractal geometry," *Comput. Vision, Graph., Image Processing*, vol. 45, pp. 150–166, 1989.
[7] T. Lundahl, W. J. Ohley, S. M. Kay, and R. Siffert, "Fractional Brownian motion: A maximum likelihood estimator and its application to image texture," *IEEE Trans. Med. Imag.*, vol. MI-5, pp. 152–161, 1986.
[8] C. C. Chen, J. S. Daponte, and M. D. Fox, "Fractal feature analysis and classification in medical image," *IEEE Trans. Med. Imag.*, vol. 8, pp. 133–142, Apr. 1989.
[9] C. M. Wu, Y. C. Chen, and K. S. Hsieh, "Texture feature for classification of ultrasonic liver images," *IEEE Trans. Med. Imag.*, vol. 11, pp. 141–152, Apr. 1992.
[10] R. C. Gonzalez and R. E. Woods, *Digital Image Processing*. Reading, MA: Addison-Wesley, 1992.
[11] D. F. Specht, "Probabilistic neural networks," *Neural Networks*, vol. 3, pp 109–118, 1990.
[12] R. M. Haralick, K. Shanmugan, and I. H. Dinstein, "Texture features for image classification," *IEEE Trans. Syst., Man, Cyber.*, vol. SMC-3, pp. 610–621, 1973.
[13] P. Burrascano, "Learning vector quantization for the probabilistic neural network," *IEEE Trans. Neural Networks*, vol. 2, pp. 458–461, 1991.

E-Liang Chen was born in Kaohsiung, Taiwan, on February 15, 1963. He received the B.S. and M.S. degrees from the Department of Electrical Engineering, National Cheng Kung University, Taiwan, in 1987 and 1993, respectively. Currently, he is a Ph.D. degree student with the Department of Electrical Engineering, National Cheng Kung University.

His current research interests are neural networks, image processing, and pattern recognition.

Pau-Choo Chung (S'89–M'91) received the B.S. and M.S. degrees in electrical engineering from National Cheng Kung University, Taiwan, Republic of China, in 1981 and 1983, respectively, and the Ph.D. degree in electrical engineering from Texas Tech University, Lubbock, in 1991.

From 1983 to 1986 she was with the Chung Shan Institute of Science and Technology, Taiwan. Since 1991, she has been with Department of Electrical Engineering of National Cheng Kung University where she is currently a Full Professor. Her current researches include neural networks and their applications to medical image processing, CT/MR image analysis, and mammography.

Ching-Liang Chen was born in Kaohsiung, Taiwan, on December 22, 1968. He received the B.S. degree in electrical engineering from Feng Chia University, Taiwan, in 1991, and the M.S. degree from the Department of Electrical Engineering, National Cheng Kung University, Taiwan, in 1993.

He is now a System Programmer with Tainan Construction Co., Taiwan.

Hong-Ming Tsai received the M.D. degree from Kaohsiung Medicine College, Taiwan, in 1985. From 1988 to 1991 he was a resident at National Cheng Kung Hospital, Taiwan.

He has been a Visiting Staff with the Department of Diagnostic Radiology of National Cheng Kung Hospital and also a Lecturer with the Department of Medicine of National Cheng Kung University since 1991 and 1993, respectively. His current research is in clinical medicine—GI radiology and interventional radiology.

Chein-I Chang (S'81–M'82–SM'92) received the B.S., M.S., and M.A. degrees from Soochow University, Taipei, Taiwan, 1973, the Institute of Mathematics at National Tsing Hua University, Hsinchu, Taiwan, 1975 and the State University of New York at Stony Brook, 1977, respectively, all in mathematics, and M.S. and M.S.E.E. degrees from the University of Illinois at Urbana–Champaign in 1982, respectively, and Ph.D. degree in electrical engineering from the University of Maryland, College Park in 1987.

He was a Visiting Assistant Professor from January 1987 to August 1987, Assistant Professor from 1987 to 1993, and is currently an Associate Professor in the Department of Computer Science and Electrical Engineering at the University of Maryland Baltimore County. He was a Visiting Specialist in the Institute of Information Engineering at the National Cheng Kung University, Tainan, Taiwan, from 1994–1995. His research interests include information theory and coding, signal detection and estimation, multispectral/hyperspectral image processing, and neural networks, pattern recognition.

Dr. Chang is a member of SPIE, INNS, Phi Kappa Phi, and Eta Kappa Nu.